LAWRENCE
LIVERMORE
NATIONAL
LABORATORY

LLNL-JRNL-411195

Raman Spectroscopy of DNA Packaging in Individual Human Sperm Cells distinguishes Normal from Abnormal Cells

T. Huser, C.A. Orme, C.W. Hollars, M.H. Corzett, R. Balhorn

March 11, 2009

Journal of Biophotonics

Disclaimer

Raman Spectroscopy of DNA Packaging in Individual Human Sperm Cells distinguishes Normal from Abnormal Cells

Thomas Huser[1,2], Christine A. Orme[3], Christopher W. Hollars[1,§], Michele H. Corzett[3], and Rod Balhorn[3]

[1]NSF Center for Biophotonics Science and Technology, University of California, Davis, Sacramento, CA 95817, USA

[2]Department of Internal Medicine, University of California, Davis, Sacramento, CA 95817, USA

[3]Physical and Life Sciences Directorate, Lawrence Livermore National Laboratory
7000 East Avenue
Livermore, CA 94551, U.S.A.

Corresponding author:
Dr. Thomas Huser, NSF Center for Biophotonics Science and Technology, and Department of Internal Medicine, University of California, Davis, Sacramento, CA 95817, USA

Ph.: (916) 734 1772, email: trhuser@ucdavis.edu

§ new address: Midwest Research Institute, 425 Volker Boulevard, Kansas City, MO 64110, U.S.A.

ABSTRACT
Healthy human males produce sperm cells of which about 25-40% have abnormal head shapes. Increases in the percentage of sperm exhibiting aberrant sperm head morphologies have been correlated with male infertility, and biochemical studies of pooled sperm have suggested that sperm with abnormal shape may contain DNA that has not been properly repackaged by protamine during spermatid development. We have used micro-Raman spectroscopy to obtain Raman spectra from individual human sperm cells and examined how differences in the Raman spectra of sperm chromatin correlate with cell shape. We show that Raman spectra of individual sperm cells contain vibrational marker modes that can be used to assess the efficiency of DNA-packaging for each cell. Raman spectra obtained from sperm cells with normal shape provide evidence that DNA in these sperm is very efficiently packaged. We find, however, that the relative protein content per cell and DNA packaging efficiencies are distributed over a relatively wide range for sperm cells with both normal and abnormal shape. These findings indicate that single cell Raman spectroscopy should be a valuable tool in assessing the quality of sperm cells for in-vitro fertilization.

KEY WORDS: Raman spectroscopy, human sperm cells, cell shape abnormalities, DNA packaging, sperm chromatin

INTRODUCTION

DNA in the testis cell, as in all other somatic cells, is packaged by histone proteins into bead-like subunits, the nucleosomes (1-3). As the testis cell begins to differentiate into sperm in mammals, a series of nuclear proteins bind to DNA and replace the majority of the histones, reorganizing the structure of the sperm chromatin complex. This process culminates when special arginine-rich proteins, the protamines, are synthesized and deposited onto the DNA, which turns off all the cell's genes (4-6)**.** These proteins neutralize the negative charge of the DNA backbone and induce its condensation into coil-like toroidal structures (7, 8). In healthy human sperm, about 10-15% of the DNA in each sperm cell remains packaged by histones and the other 85-90% are packaged by protamines. This reorganization in sperm genome packaging is essential for the reproduction cycle because it inactivates the majority of the spermatid's genes and sets the stage for the introduction of the male genome into the egg.

Sperm cells from 50-70% of all infertile males, however, contain improperly packaged DNA (9) and the majority of sperm produced by many infertile males have abnormally shaped heads (10)**.** Even in healthy individuals a significant number of sperm cells (25-40%) have heads with abnormal shape and are believed to be dysfunctional. While there are many factors that may contribute to the production of sperm with abnormal head shapes, a number of studies have provided evidence that abnormal sperm may be linked to improperly packaged chromatin (9, 11-14)**.** Sperm head morphology has been established by the World Health Organization (WHO) as the most important criterion to assess the fertility of males. There is, however, evidence and growing concern that not all sperm with normal shape are fully functional and may contain DNA that is improperly packaged (15-17). Fertilization events involving abnormal sperm could have adverse effects on early embryo development or lead to genetic disease. Thus, the development of a technique that can noninvasively probe the efficiency of DNA packaging in living sperm cells in-vivo would be of great value.

Most analytical techniques with high spatial resolution, such as analytical electron microscopy, X-ray imaging, or secondary ion-mass spectroscopy, to name a few, destroy the sample during the analysis or cannot be used to examine living cells without inducing damage. If these techniques are used to assess the quality of sperm cells the cells cannot subsequently be used for in-vitro fertilization. Micro-Raman spectroscopy on the other hand offers promise to provide information about DNA packaging at the single sperm cell level for living cells. It can be used to obtain images of the cell's shape together with a chemical analysis of the cell's contents. Raman spectroscopy examines the inelastic scattering of photons by molecular bonds, where the scattered photons can either lose part of their energy and are red-shifted ("Stokes"-shifted) or gain energy and are blue-shifted ("anti-Stokes"-shifted). Raman spectroscopy has recently become more popular in the life sciences with the advent of new, more powerful and reliable laser sources and more sensitive light detectors (18). This technique is mostly noninvasive and nondestructive at moderate photon energies and works *in vitro* and *in vivo* under a wide range of environmental conditions. It offers detailed information about the conformation, composition and intermolecular interactions of macromolecules such as DNA and proteins (19-21)**.** The first report in the literature of a single-cell Raman analysis was in

fact conducted on individual living salmon sperm cells that were investigated within the cavity of a high-power laser system (22). Shortly thereafter it was shown, that if combined with confocal laser microscopy, Raman spectroscopy can be used to obtain information from individual living cells even with subcellular resolution (18). Since then, the applications of Raman spectroscopy to single cells have grown exponentially (23, 24), and applications related to single cancer cells (25), human embryonic stem cells (26), and even biological particles as small as lipoproteins (27) and bacterial spores (28) have been demonstrated. In addition, the field of coherent Raman microscopy has emerged, which enables label-free imaging of individual cells and tissues in vitro and in vivo (23, 24, 29-32).

Here, we have examined the spectra obtained from single sperm cells of a healthy human individual by micro-Raman spectroscopy in an effort to determine if there are DNA or protein related differences in the Raman spectra of sperm chromatin that correlate the shape of the nucleus (normal vs. abnormal) with protein content and DNA conformation. While the current study was conducted on fixed cells in order to minimize sample handling issues during optimization of the technical procedures, this analysis can easily be extended to living cells. This can, for example, be facilitated by the combination of laser tweezers and Raman spectroscopy or the rapid analysis of cells by coherent Raman techniques (23, 24).

MATERIALS AND METHODS

Sample preparation

Human semen was obtained from a healthy donor, distributed into aliquots and frozen. Aliquots of sperm from this same individual have been examined previously by PIXE (Proton Induced X-ray Emission) and XANES (X-ray Absorption Near Edge Structure) to assess the DNA, protein and zinc content of individual sperm heads (33-35). An aliquot of semen was thawed, washed three times by suspending in 0.01M Tris pH8, 0.15M sodium chloride (T/S) with brief sonication and sedimented by centrifugation for 3 minutes at 4000g. The cells were resuspended in water and applied to quartz coverslips for analysis.

All data shown in this article were obtained from cells that were treated to have their membranes and tails removed. This treatment was deemed necessary to obtain Raman spectra from the pure nuclear DNA-protein complex without potentially interfering contributions from membrane proteins. Later in the investigation, after analyzing the data obtained from treated cells we compared these Raman spectra to those obtained from fixed whole cells and found no significant differences (data not shown). To prepare sperm heads lacking their membranes and tails, the washed sperm were treated with 10mM dithiothreitol (DTT), 0.01M Tris pH8, and 1% mixed alkyl trimethylammonium bromide (MTAB) for 1 hour at 4°C to dissolve the tails and membranes, followed by centrifugation at 4000g for 3 min. The nuclear pellet was washed two times in 1% CTAB, 0.01M Tris pH 8. The resulting amembranous sperm heads contain only the DNA-protein complex that comprises sperm chromatin. After rinsing in distilled water, the amembraneous sperm heads were then resuspended in deionized water. This treatment of the samples does not alter the morphology of the sperm head (36). Each of

the sperm head morphology classes reported previously by Moruzzi et al. (37) can still be identified and distinguished (36).

To prepare the sperm samples for Raman analysis, amembraneous sperm nuclei were allowed to adsorb to 25mm diameter circular quartz cover slips for several minutes after depositing an aliquot of the treated sperm cell suspension onto the quartz, and the coverslips were then rinsed with deionized water and used for analysis immediately thereafter. This resulted in a typical coverage of about 1 sperm cell per 100 μm^2.

A DNA gel was prepared as a reference sample by dissolving cesium chloride gradient purified calf thymus DNA in 10mM Tris, 0.1mM EDTA at a concentration of 10mg/ml. Raman spectra were obtained by depositing a 20µl droplet of the gel on circular quartz coverslips and focusing the laser beam into the gel.

Experimental Setup

The confocal micro-Raman setup uses the 488 nm line of a 50 mW air-cooled argon-ion laser as excitation source. While 488 nm laser light has been used extensively in bulk Raman spectroscopy, its application to micro-Raman spectroscopy is typically not beneficial, since it can result in significant spectral modifications and background fluorescence (38). This was essential in our application to enable us to compare autofluorescence maps providing accurate size-measurements of the cells with the resulting Raman spectra. This was made possible by the robustness of sperm cells and the relatively low power used in this study. For live cell applications, this work will require the use of near-infrared laser wavelengths. The beam of the 488 nm laser is passed through a narrow bandpass filter to remove residual laser plasma lines and is then coupled into the rear entrance port of an upright optical microscope (Diaphot, Nikon). A pellicle beamsplitter reflects the laser beam towards an objective lens with 100x magnification and super-long working distance (SLWD, 100x, NA 0.73, Nikon) that focuses the light to a diffraction-limited spot at the sample. The same microscope objective is used to collect and collimate the Stokes-shifted spontaneous Raman-scattered light. After passing the beamsplitter, the light is focused through a confocal pinhole with 100 µm diameter using the microscope tube lens. The light is then collimated by a single antireflection-coated achromatic lens and passed through a holographic notch filter (HSPF-488-1, Kaiser Optical) that efficiently blocks the excitation light. It is then focused to the entrance slit (100 µm slit width) of an imaging monochromator (Triax 320, SPEX JY Horiba) that disperses the light onto a liquid nitrogen cooled back-thinned charge coupled device camera (LN/CCD-1340/100, Princeton Instruments). Light dispersion is achieved by a 1200 lines/mm diffraction grating which results in a spectral resolution of ~4 cm^{-1}. The sample is held on a closed-loop controlled three-axis piezo scan stage (P-517.3CL, Physik Instrumente) with a scan range of 100 µm x 100 µm x 20 µm (xyz). All spectra are calibrated against a toluene standard (does this need a reference?).

In a typical experimental run, samples are first imaged at low power by building up images of their autofluorescence pixel by pixel within a total image acquisition time of 2.5 min for 256x256 pixels. These images are stored on a personal computer for further

analysis and the laser beam is then positioned over specific parts of the cells according to these fluorescence images. Just before the acquisition of Raman spectra the sample autofluorescence was pre-bleached for about 1 min. at 1 mW laser power, which corresponds to a local power density of about 100kW/cm^2. All spectra are corrected for the quartz glass Raman spectrum by subtracting a quartz background spectrum. Raman spectra of individual cells are accumulated for 5 minutes at a power density of 100kW/cm^2. At this laser power, no photo-induced degradation is observed in the sample (data not shown) (39). One should note, however, that this is attributed to the robustness of the amembraneous sperm cells and is not transferrable to the analysis of living cells (38). In addition to subtracting the quartz background, all spectra are also post-processed by subtracting a 5th order polynomial that fits the residual broad fluorescence background and then normalized to the DNA backbone vibration at 1092 cm^{-1}. All spectra are treated in exactly the same way to ensure accurate comparison of Raman peak intensities. All images of sperm cells are sorted into 10 different head shape classes according to the sperm morphology criteria of Moruzzi et al. (37). This classification was repeated blindly 3 times and only cells that had a positive correlation with the same shape class in at least 2 of the 3 runs are used for further analysis.

RESULTS

Figure 1 shows a typical confocal autofluorescence image of two sperm cell nuclei immobilized on a quartz coverslip (Fig. 1a) along with the Raman spectrum of sperm head A (Fig. 1b) and the Raman spectrum of calf-thymus DNA (Fig. 1c) in the 600 – 1800 cm^{-1} fingerprint region. The head of sperm cell A in Fig. 1a was classified as normal, while the head of cell B was classified as pear-shaped using the criteria described by Moruzzi et al. (37). According to criteria established by the WHO, a typical normal sperm cell has an oval head shape with a well-defined acrosomal region covering 40-70% of the head. The head has a typical length of 4 - 5.5 μm, a width of 2.5 - 3.5 μm and a length-to-width ratio of 1.5 - 1.75. The distribution of the autofluorescence intensity within sperm head A in Figure 1a is given by the local cell thickness and correlates well with atomic force microscope images of individual sperm cells (40). The acrosomal region in each cell is characterized by a weaker autofluorescence because of its significantly lower thickness. The spectrum obtained from this cell (cf. Fig. 1b) is the characteristic Raman spectrum of a sperm head with normal shape obtained from the central part of the head. It has an excellent signal-to-noise ratio and reveals all the vibrational bands of a typical Raman spectrum of a DNA-protein complex (41). Repeated acquisition of spectra from the same cell resulted in excellent reproducibility of the spectra with negligible variation. The calf-thymus DNA gel spectrum in Fig. 1c exhibits the same overall characteristics as a Raman spectrum of DNA with 42% guanine and cytosine content (42). For our applications, the most relevant peaks in this spectrum are the strong Raman peak at 785 cm^{-1} which has contributions from tyrosine and cytosine vibrations as well as from the DNA backbone, the PO_2^- backbone vibration at 1092 cm^{-1}, the deoxyadenine (dA) vibration at 1302 cm^{-1}, and the deoxyguanine (dG) vibration at 1315 cm^{-1}. For a complete assignments of all peaks see table I. The sperm cell spectrum (Fig. 1b) is characterized by a much weaker peak at 785 cm^{-1}, and a strong methylene

deformation mode at 1442 cm^{-1} as well as additional contributions to the 1300 cm^{-1} and 1335 cm^{-1} peaks, all due to protein CH_2 twisting vibrations.

The spatial resolution of our micro-Raman instrument (~1μm) allows us to obtain Raman spectra from different parts of a cell with subcellular resolution. This is demonstrated in Figure 2, where we compare Raman spectra obtained from different parts of a human sperm head with normal morphology. The Raman spectra shown in Fig. 2b were obtained from the lower part of the sperm head (right above the tail in an intact cell) (A), the mid-section (B) and the acrosomal part of the sperm head (C). Raman bands and intensities reproduce very well for all three regions, providing evidence that there cannot be major regional differences in the DNA-protein content within the same normal-shaped sperm head within the ~ 1 femtoliter probe volume of our confocal micro-spectroscopy setup.

In Figure 3 characteristic spectra of sperm heads from different shape classes are shown along with representative images of the sperm heads. Fig. 3a is the averaged spectrum of 4 pear-shaped sperm heads with a representative shown in Fig. 3b. Fig. 3c is the averaged spectrum of 4 small sperm heads, together with a typical image (Fig. 3d). Fig. 3e shows the averaged spectrum of 3 sperm heads from the shape class “double” along with a typical image in Fig. 3f. Fig. 3g is the averaged spectrum of 11 normal sperm heads, again with a typical autofluorescence image shown in Fig. 3h. All spectra were obtained from the central section of each sperm head.

In Figure 4 we compare Raman spectra of 4 sperm heads that were all identified as having normal shape. Note the differences in the intensities of the cytosine ring vibration at 785 cm^{-1} and the protein methylene deformation mode at 1442 cm^{-1} between different sperm heads.

DISCUSSION

The Raman spectrum of the normal human sperm cell in Fig. 1b as compared to the calf-thymus DNA in Fig. 1c exhibits some striking differences. These clearly identify the source of the Raman spectrum of the sperm head as a DNA-protein complex and provide important information about the packaging of the DNA inside the sperm head. First, and most notably, both spectra have a strong guanine ring breathing mode at 680 cm^{-1}, which indicates that their sugar-phosphate backbone is in B-form conformation (43). The 728 cm^{-1} adenine vibrational band is slightly enhanced in the sperm head, which indicates that adenine in the sperm cell is somewhat unstacked. This feature is very similar to that obtained in the Raman spectrum of a DNA melting process, which is characterized by a helix to coil transition (44). This is in good agreement with an earlier Raman study of artificial protamine-DNA complexes (41). The combined phosphodiester backbone stretch and cytosine breathing modes at 785 cm^{-1} are significantly suppressed in the sperm spectrum. This indicates strong electrostatic binding of the proteins close to the DNA phosphates (45) and is consistent with the crosslinking of the two DNA strands by adjacent arginine residues in the DNA binding domain of the bound protamine (41, 46). Surprisingly, this peak is significantly more suppressed in the sperm spectrum than in artificial protamine-DNA complexes (41). This provides evidence that the natural protein-assisted packaging of DNA achieved during spermatid development may produce

a more uniformly and tightly compacted DNA-protein complex than is achieved by adding protamine to DNA *in vitro*. The presence of the protein appears to have no effect on the 1092 cm^{-1} PO_2^- band of the DNA backbone, which thus provides a good means for intensity calibration. The absence of an 807 cm^{-1} band in the sperm spectrum also indicates the complete absence of any A-form backbone conformation (41).

Other noticeable differences between the pure DNA and sperm spectra are a significant increase in the adenine band at 1302 cm^{-1} and a moderate increase in the band at 1335 cm^{-1}. Both receive contributions from a broad protein CH_2 twisting mode centered at 1320 cm^{-1}. The strong adenine vibration at 1420 cm^{-1} in the calf-thymus DNA spectrum is just a slight shoulder on the dominating methylene deformation mode of the proteins at 1442 cm^{-1}. This, together with the increased peaks around 1300 cm^{-1} and 1665 cm^{-1} are the most striking bands, which reveal the presence of proteins in the sperm head spectrum. Again, all these bands are significantly stronger in intensity than in artificial protamine-DNA complexes, which indicates a higher protein concentration and thus more efficient or complete protein complexation of DNA in sperm. Finally, the deoxynucleoside band at 1665 cm^{-1} obtains additional contributions from the protein amide I band, which shifts the peak position to 1670 cm^{-1}.

The Raman spectra obtained from sperm chromatin packed inside the heads of normal sperm cells indicate that DNA is very efficiently packaged by protamines that bind to the major groove of DNA and slightly unstack the DNA bases. An indicative marker of the efficiency of the packaging process appears to be the intensity of the 785 cm^{-1} band, where a low intensity indicates highly efficient protein binding. The relative amount of protein present within the sperm nucleus can be obtained from the peak strength of the 1442 cm^{-1} methylene deformation mode. The ribophosphate backbone vibration at 1092 cm^{-1} and the 1575 cm^{-1} peak from the purine bases appear to be relatively unaffected by protein binding. We chose to use the DNA backbone vibration at 1092 cm^{-1} as an independent marker mode in order to quantitatively describe the degree of DNA-protein complexation and normalized all spectra with respect to this peak. This peak appeared to be the least affected by protamine binding to the DNA. The ratio between the strengths of the 1442 cm^{-1} band and this backbone vibration then provides an accurate measure for the relative proportion of DNA and protein (DNA-protein ratio) present in the sperm nucleus.

As demonstrated in Figure 2, we observed little to no spatial variation among the Raman spectra obtained from the same sperm head with normal shape. This indicates a homogeneous distribution of the protein content within the nucleus and the same spatial efficiency of DNA packaging. This is in agreement with earlier results that mapped the protein and DNA distribution within bull sperm cells by high-resolution X-ray imaging (33). Regardless, all averaged spectra shown in this article were acquired from the central region of the cells.

Out of a total of 50 cells that we studied, 28 could clearly be classified into shape classes and their spectra had acceptable signal-to-noise ratios. The remaining 22 cells could either not be classified with confidence or their spectra had very poor signal-to-noise ratios. Among the 17 cells that were classified as abnormal, the shape classes of pear,

small, double, round, and narrow had at least 3-4 cells in each class that would allow us to average their Raman spectra within each class. This is demonstrated in Figure 3 for three of the abnormal categories and they are listed in comparison with the averaged spectrum of 11 cells with normal shape. The comparison of the Raman spectra from sperm cells with different abnormal shapes as presented in Fig. 3 shows that the overall protein content as observed by the intensity of the 1442 cm^{-1} peak varies significantly between classes. A more significant observation, however, is the fact that all cells that were classified as abnormal appear to have less efficient DNA packaging than the normal cells as evidenced by the peak strengths at 785 cm^{-1}. We can express this more quantitatively by assuming that the 785 cm^{-1} peak strength of the DNA gel (Fig. 1c) describes the case where no protein is bound to DNA. In this case, the relative peak strength compared to the intensity of the 1092 cm^{-1}backbone vibration is 1.61. We further assume that the averaged Raman spectrum of all normal cells (Fig. 3g) describes the case where DNA is completely complexed with proteins, and its peak strength is 0.56, respectively. If we then use the approximation that the peak strength of the 785 cm^{-1} peak is proportional to the relative amount of protein bound to DNA, an average peak height of 0.74 for pear-shaped cells, 0.72 for small cells, and 0.73 for double-shaped cells suggests that DNA-protein complexation is on average 15 - 17% less efficient in these abnormal cells. This difference may be related to the presence of increased amounts of other proteins (e.g. histones, transition proteins, variation in protamine P2 content) bound to DNA in these sperm. These proteins bind more loosely to the DNA than protamines and are less effective in suppressing DNA vibrations related to the phosphodiester backbone or cytosine breathing mode. Such differences in protein content have been suggested by others based on analyses of pools of sperm obtained from infertile individuals (9). Variations in the total protein content of each sperm cell will result in a change of the relative intensity of the 1442 cm^{-1} protein deformation peak. As summarized in Table 2, the intensity of this peak varies between cells with different shape, but it is never significantly reduced compared to the normal cells, which indicates a similar or even higher protein content in the abnormal cells. This observation supports the potential presence of other proteins.

In Figure 4 we compare the Raman spectra of four sperm cells with normal shape. According to the 1442 cm^{-1} peak intensities the relative protein content in these cells varies significantly from 1.10 (Fig. 4a) to 1.49 (Fig. 4d). Among the total of eleven cells with normal shape, we observe a distribution of the relative protein content between 0.9 and 1.5. Similarly, the peak intensity of the 785 cm^{-1} band varies between 0.48 and 0.7, indicating a variation in the efficiency of DNA packaging in these cells. The majority of the eleven normal sperm cells have peak ratios relatively close to the average (Fig. 3g), but a few cells have peak ratios that are closer to that of the abnormal cells. This observation is consistent with previous dye binding studies of human sperm considered to have a normal head shape morphology (16). This finding is extremely important. Currently clinicians selecting sperm for ICSI and other assisted fertilization methods using single sperm cells pick the sperm to be introduced into the eggs based primarily on their morphology, and in some cases a combination of morphology and motility. The Raman results, as well as the dye binding studies reported earlier (16), indicate that the

population of sperm with normal head shapes is clearly heterogeneous in composition, and they may also be variable in their functionality.

In summary, we have provided Raman-spectroscopic evidence obtained from analyses of individual cells that indicates that DNA packaging in human sperm cells with abnormal shape is different than in sperm with normal shape. Since abnormally shaped sperm are generally believed to be dysfunctional (as the number of sperm with head shape abnormalities increases, the fertility of the male decreases (10, 47, 48)), the results of the Raman studies suggest that differences in the packaging of DNA in normal and abnormal sperm may contribute to deficiencies in abnormal sperm function following fertilization. More importantly, however, we also find that the nature and efficiency of DNA packaging in sperm considered having normal head shape morphologies appears to vary greatly. Thus, by selecting sperm cells solely based on shape, a significant fraction of the "normal" sperm cells clinicians pick for use in *in vitro* fertilization will contain improperly packaged DNA. It is clear, that more statistics are needed to make more definitive statements, which can be achieved by higher throughput techniques. We can e.g. envision a combined flow-cytometer and Raman spectrometer, which would use a laser-trap to hold living sperm cells combined with a near-infrared laser to probe their Raman spectrum. The cells could then be sorted into shape-classes by computer-assisted image analysis (37) and their Raman spectra be processed and used as an additional means of evaluating the "quality" of the each sperm's genome and selecting those cells for use in assisted fertilization. Laser trapping is already widely used and is beginning to be accepted as a technique for use in *in-vitro* fertilization (49). The addition of Raman spectroscopy could be a rather simple but very beneficial step. By combining this with coherent Raman techniques, such as coherent anti-Stokes Raman scattering (CARS) (23, 24, 29, 31) or stimulated Raman scattering (SRS) (30, 32) even fast flow schemes analyzing thousands of cells will be possible, which is further aided by the spatial uniformity of Raman spectra in sperm cells.

ACKNOWLEDGMENTS

This work was supported by the Laboratory Directed Research and Development Program of Lawrence Livermore National Laboratory under the auspices of the U.S. Department of Energy by Lawrence Livermore National Laboratory under Contract DE-AC52-07NA27344.

REFERENCES

1. Morales V, *et al*. (2001) Chromatin structure and dynamics: Functional implications. *Biochimie* 83(11-12):1029-1039.
2. Hayes JJ & Hansen JC (2001) Nucleosomes and the chromatin fiber. *Curr Opin Genet Dev* 11(2):124-129.
3. Kornberg RD & Lorch Y (1999) Twenty-five years of the nucleosome, fundamental particle of the eukaryote chromosome. *Cell* 98(3):285-294.
4. Goldberg RB, Geremia R, & Bruce WR (1977) Histone synthesis and replacement during spermatogenesis in the mouse. *Differentiation* 7(3):167-180.
5. Bellve AR (1979) *The Molecular Biology of Mammalian Spermatogenesis*, ed Finn CA (Oxford Univ. Press, London), Vol 1, pp 159-261.
6. Braun RE (2001) Packaging paternal chromosomes with protamine. *Nat Genet* 28(1):10-12.
7. Allen MJ, *et al*. (1993) Analysis of Synthetic Dnas and DNA-Protamine Complexes with the Scanning Tunneling Microscope. *Scanning Microscopy* V7(N2):563-576.
8. Balhorn R, *et al*. (1999) Protamine Mediated Condensation of DNA in Mammalian Sperm. *The Male Gamete: From Basic Knowledge to Clinical Applications*, ed Gagnon C (Cache River Press, Vienna, IL), pp 55-70.
9. de Yebra L, Ballesca JL, Vanrell JA, Bassas L, & Oliva R (1993) Complete selective absence of protamine P2 in humans. *J Biol Chem* 268(14):10553-10557.
10. MacLeod J (1951) Semen quality in one thousand men of known fertility and in eight hundred cases of infertile marriage. *Fert Steril* 2:115.
11. Balhorn R, Reed S, & Tanphaichitr N (1988) Aberrant protamine 1/protamine 2 ratios in sperm of infertile human males. *Experientia* 44(1):52-55.
12. Blanchard Y, Lescoat D, & Le Lannou D (1990) Anomalous distribution of nuclear basic proteins in round-headed human spermatozoa. *Andrologia* 22(6):549-555.
13. Bach O, Glander HJ, Scholz G, & Schwarz J (1990) Electrophoretic patterns of spermatozoal nucleoproteins (NP) in fertile men and infertility patients and comparison with NP of somatic cells. *Andrologia* 22(3):217-224.
14. Belokopytova IA, Kostyleva EI, Tomilin AN, & Vorob'ev VI (1993) Human male infertility may be due to a decrease of the protamine P2 content in sperm chromatin. *Mol Reprod Dev* 34(1):53-57.
15. Angelopoulos T, *et al*. (1998) Simultaneous assessment of sperm chromatin condensation and morphology before and after separation procedures: effect on the clinical outcome after in vitro fertilization. *Fertil Steril* 69(4):740-747.
16. Hofmann N & Hilscher B (1991) Use of aniline blue to assess chromatin condensation in morphologically normal spermatozoa in normal and infertile men. *Hum Reprod* 6(7):979-982.
17. Schlicker M, Schnulle V, Schneppel L, Vorob'ev VI, & Engel W (1994) Disturbances of nuclear condensation in human spermatozoa: search for mutations in the genes for protamine 1, protamine 2 and transition protein 1. *Hum Reprod* 9(12):2313-2317.

18. Puppels GJ, *et al*. (1990) Studying Single Living Cells and Chromosomes by Confocal Raman Microspectroscopy. *Nature* V347(N6290):301-303.
19. Peticolas WL (1995) Raman spectroscopy of DNA and proteins. *Methods Enzymol* 246:389-416.
20. Peticolas WL & Evertsz E (1992) Conformation of DNA in vitro and in vivo from laser Raman scattering. *Methods Enzymol* 211:335-352.
21. Koenig JL (1972) Raman spectroscopy of biological macromolecules: A review. *Journal of Polymer Science D*:59-177.
22. Kubasek WL, *et al*. (1986) Raman Spectra of the Model B-DNA Oligomer $d(CGCGAATTCGCG)_2$ and of the DNA in Living Salmon Sperm Show That Both Have Very Similar B-Type Conformations. *Biochemistry-USA* 25:7440-7445.
23. Chan J, Fore S, Wachsmann-Hogiu S, & Huser T (2008) Raman spectroscopy and microscopy of individual cells and cellular components. *Laser & Photon Rev* 2(5):325 – 349.
24. Wachsmann-Hogiu S, Weeks T, & Huser T (2009) Chemical analysis in vivo and in vitro by Raman spectroscopy — from single cells to humans. *Curr Opin Biotechnol* in print.
25. Chan JW, *et al*. (2006) Micro-Raman Spectroscopy Detects Individual Neoplastic and Normal Hematopoietic Cells. *Biophys. J*. 90(2):648–656.
26. Chan JW, Lieu DK, Huser T, & Li RA (2009) Label-Free Separation of Human Embryonic Stem Cells and Their Cardiac Derivatives Using Raman Spectroscopy. *Anal Chem* 81(4):1324–1331.
27. Chan JW, Motton D, Rutledge JC, Keim NL, & Huser T (2005) Raman spectroscopic analysis of biochemical changes in individual triglyceride-rich lipoproteins in the pre- and postprandial state. *Anal Chem* 77(18):5870-5876.
28. Chan JW, *et al*. (2004) Reagentless identification of single bacterial spores in aqueous solution by confocal laser tweezers Raman spectroscopy. *Anal Chem* 76(3):599-603.
29. Zumbusch A, Holtom GR, & Xie XS (1999) Three-dimensional vibrational imaging by coherent anti-Stokes Raman scattering. *Physical Review Letters* 82(20):4142-4145.
30. Ploetz E, Laimgruber S, Berner S, Zinth W, & Gilch P (2007) Femtosecond stimulated Raman microscopy. *Appl. Phys. B* 87:389–393.
31. Xie XS, Yu J, & Yang WY (2006) Perspective - Living cells as test tubes. (Translated from English) *Science* 312(5771):228-230 (in English).
32. Freudiger CW, *et al*. (2008) Label-Free Biomedical Imaging with High Sensitivity by Stimulated Raman Scattering Microscopy *Science* 322:1857-1861.
33. Zhang XD, Balhorn R, Mazrimas J, & Kirz J (1996) Measuring DNA to Protein Ratios in Mammalian Sperm Head by Xanes Imaging. *J Struct Biol* V116(N3):335-344.
34. Bench GS, Friz AM, Corzett MH, Morse DH, & Balhorn R (1996) DNA and Total Protamine Masses in Individual Sperm from Fertile Mammalian Subjects. *Cytometry* V23(N4):263-271.

35. Bench G, Corzett MH, Kramer CE, Grant PG, & Balhorn R (2000) Zinc is sufficiently abundant within mammalian sperm nuclei to bind stoichiometrically with protamine 2. *Mol Reprod Dev* V56(N4):512-519.
36. Lee JD, Allen MJ, & Balhorn R (1997) Atomic force microscope analysis of chromatin volumes in human sperm with head-shape abnormalities. *Biol Reprod* V56(N1):42-49.
37. Moruzzi JF, Wyrobek AJ, Mayall BH, & Gledhill BL (1988) Quantification and classification of human sperm morphology by computer-assisted image analysis. *Fert Steril* 50:142-152.
38. Puppels GJ, *et al*. (1991) Laser irradiation and Raman spectroscopy of single living cells and chromosomes: Sample degradation occurs with 514.5 nm but not with 660 nm laser light. *Exp Cell Research* 195(2):361-367.
39. Puppels GJ, *et al*. (1991) Laser Irradiation and Raman Spectroscopy of Single Living Cells and Chromosomes - Sample Degradation Occurs with 514.5nm but Not with 660nm Laser Light. *Experimental Cell Research* V195(N2):361-367.
40. Allen MJ, *et al*. (1993) Atomic Force Microscopy of Mammalian Sperm Chromatin. *Chromosoma* V102(N9):623-630.
41. Hud NV, Milanovich FP, & Balhorn R (1994) Evidence of Novel Secondary Structure in DNA-Bound Protamine Is Revealed by Raman Spectroscopy. *Biochemistry-USA* V33(N24):7528-7535.
42. Deng H, Bloomfield VA, Benevides JM, & Thomas GJ (1999) Dependence of the raman signature of genomic B-DNA on nucleotide base sequence. *Biopolymers* V50(N6):656-666.
43. Benevides JM & Thomas GJ (1983) Characterization of DNA Structures by Raman-Spectroscopy - High-Salt and Low-Salt Forms of Double Helical Poly(Dg-Dc) in H2o and D2o Solutions and Application to B-DNA, Z-DNA and a-DNA. *Nucl Acid Res* 11(16):5747-5761.
44. Erfurth SC & Peticolas WL (1975) Melting and Premelting Phenomenon in DNA by Laser Raman- Scattering. *Biopolymers* 14(2):247-264.
45. Deng H, Bloomfield VA, Benevides JM, & Thomas GJ (2000) Structural basis of polyamine-DNA recognition: spermidine and spermine interactions with genomic B-DNAs of different GC content probed by Raman spectroscopy. *Nucl Acid Res* V28(N17):3379-3385.
46. Balhorn R (1989) Mammalian Protamines: Structure and Molecular Interactions. *Molecular Biology of Chromosome Function*, ed Adolph KW (Springer-Verlag, New York), p 366.
47. Kullander S & Rausing A (1975) On round-headed human spermatozoa. *Int J Fertil* 20(1):33-40.
48. Kruger TF, *et al*. (1986) Sperm morphologic features as a prognostic factor in in vitro fertilization. *Fertil Steril* 46(6):1118-1123.
49. Schutze K, Clement-Sengewald A, & Ashkin A (1994) Zona drilling and sperm insertion with combined laser microbeam and optical tweezers. *Fert Steril* 61(4):783-786.

Table I: Raman frequencies and their assignments

Raman frequency in wavenumber units (cm^{-1})	Assignment[a]
642	dC
670	dT
681	dG
728	dA
785	dT, dC, bk
831	νOPO
890	d
960	d
1053	νCO
1092	νPO_2^-
1213	dC, dT
1237	dT, dC
1255	dA, dC
1292	dC
1302	dA
1315	dG
1335	dA, dG
1374	dT, dA, dC
1420	dA
1442	$d(CH_2\delta)$
1484	dG, dA
1575	dG, dA
1665 (broad)	dC, dG, dA, dT

[a] Abbreviations: ν and δ indicate stretching and deformation vibrations, respectively. bk indicates a vibration of the DNA backbone; d indicates a vibration localized in the deoxyribose moiety; C, T, A, G are DNA bases. See text for more details. Assignments are based on (18, 19, 41-44).

Table II: Peak intensities relative to the DNA backbone vibration for different cell shape classes

	Normal	Pear	Small	Double
I (785 cm^{-1}) / I (1092 cm^{-1})	0.56	0.74	0.72	0.73
I (1442 cm^{-1}) / I (1092 cm^{-1})	1.18	1.42	1.15	1.26

Figure captions

Fig. 1: (a) Confocal autofluorescence image of a normal human sperm cell head (A) and a pear-shaped sperm cell head (B) immobilized on a quartz optical flat. (b) Spontaneous micro-Raman spectrum of the central part of the normal sperm head A. (c) Spontaneous micro-Raman spectrum of calf-thymus DNA gel. Raman peaks with the most significant differences for this study are highlighted by gray shades.

Fig. 2: (a) Confocal autofluorescence image of a normal human sperm cell head immobilized on a quartz optical flat. (b) Raman spectra obtained from the tail region (A), the mid-section (B) and the acrosomal region (C) of the cell.

Fig. 3: Raman spectra and autofluorescence micrographs of human sperm cells from different cell classes. (a), (b) pear-shaped cells, (c), (d) small cells, (e), (f) double cells, and (g), (h) normal sperm cells. Note the variations in peak intensities at the highlighted positions, which indicate differences in DNA packaging efficiency and relative protein content.

Fig. 4: Spontaneous Raman spectra from the central part of 4 individual human sperm heads with normal shape. Protein-DNA ratios were measured by comparing the intensity of the 1442 cm^{-1} methylene deformation mode to the intensity of the 1092 cm^{-1} DNA backbone vibration. (a) Protein-DNA ratio: 1.10. (b) Protein-DNA ratio: 1.21. (c) Protein-DNA ratio: 1.30. (d) Protein-DNA ratio: 1.49. Note the variations in peak intensities at the highlighted positions, which indicate differences in DNA packaging efficiency and relative protein content.

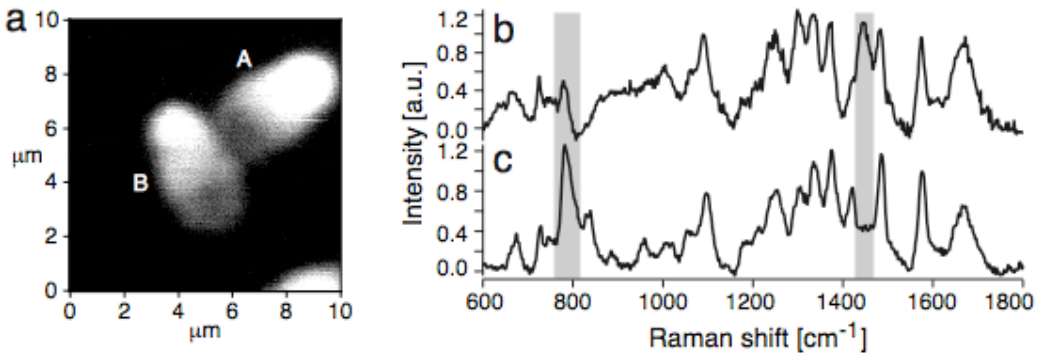

Huser et al., Figure 1

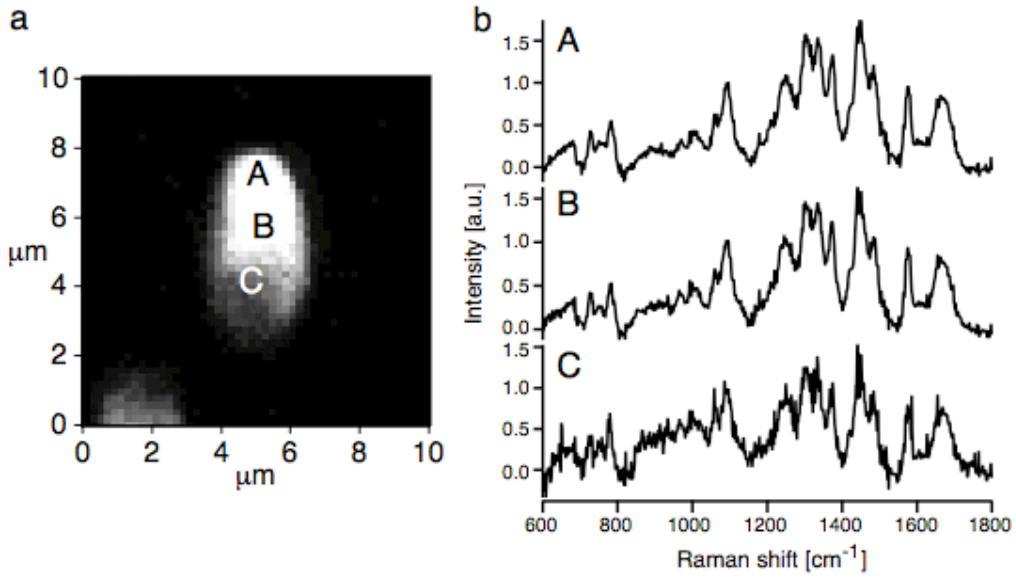

Huser et al., Figure 2

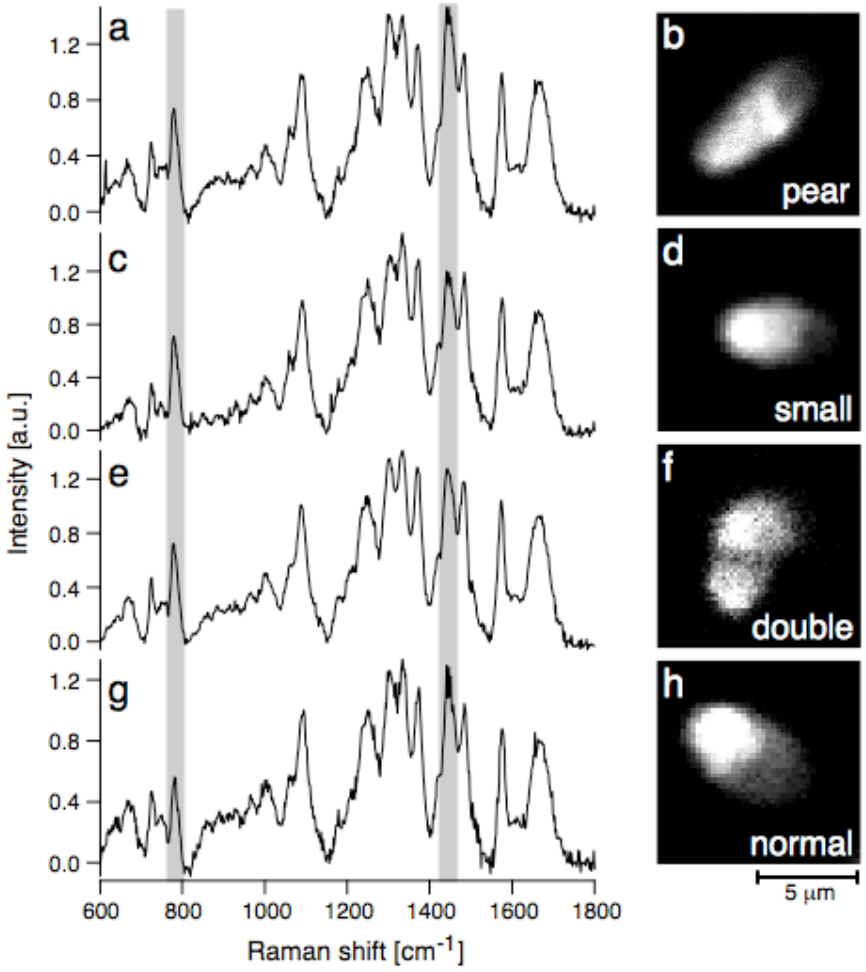

Huser et al., Figure 3

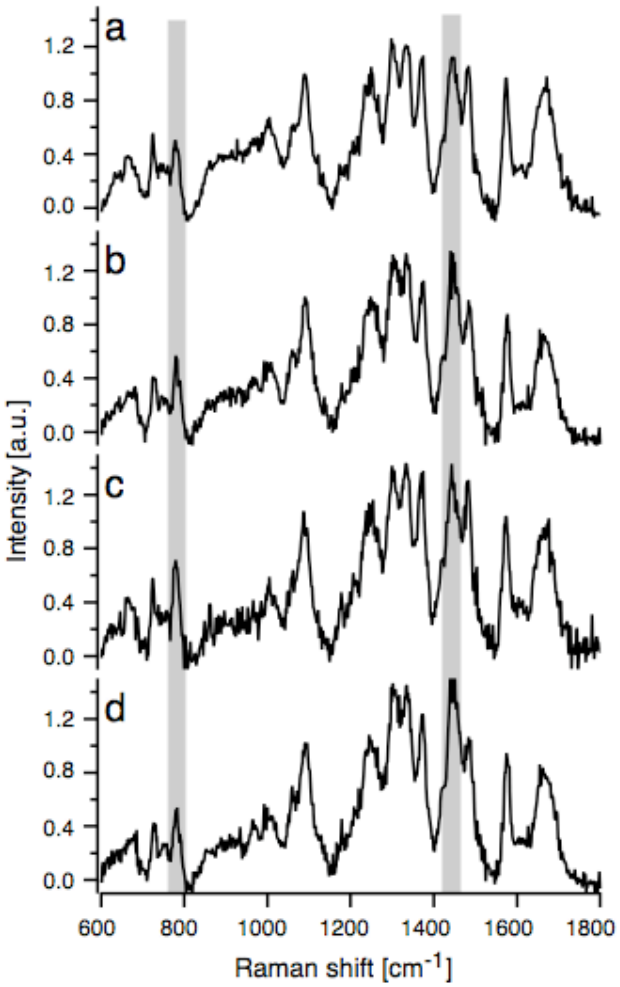

Huser et al., Figure 4